Physics Letters A 380 (2016) 1772–1780

Contents lists available at ScienceDirect

Physics Letters A

www.elsevier.com/locate/pla

Topological map of the Hofstadter butterfly: Fine structure of Chern numbers and Van Hove singularities

Gerardo G. Naumis [a,b,c,*]

[a] Departamento de Física–Química, Instituto de Física, Universidad Nacional Autónoma de México (UNAM), Apartado Postal 20-364, 01000 México, Distrito Federal, Mexico
[b] Department of Physics and Astronomy, George Mason University, Fairfax, VA 22030, USA
[c] Escuela Superior de Física y Matemáticas, ESIA-Zacatenco, Instituto Politécnico Nacional, México D.F., Mexico

ARTICLE INFO

Article history:
Received 29 July 2015
Received in revised form 24 February 2016
Accepted 14 March 2016
Available online 17 March 2016
Communicated by R. Wu

Keywords:
Quantum Hall effect
Chern numbers
Topological phases
Quasicrystals
Hofstdater butterfly
Van Hove singularities

ABSTRACT

The Hofstadter butterfly is a quantum fractal with a highly complex nested set of gaps, where each gap represents a quantum Hall state whose quantized conductivity is characterized by topological invariants known as the Chern numbers. Here we obtain simple rules to determine the Chern numbers at all scales in the butterfly fractal and lay out a very detailed topological map of the butterfly by using a method used to describe quasicrystals: the cut and projection method. Our study reveals the existence of a set of critical points that separates orderly patterns of both positive and negative Cherns that appear as a fine structure in the butterfly. This fine structure can be understood as a small tilting of the projection subspace in the cut and projection method and by using a Chern meeting formula. Finally, we prove that the critical points are identified with the Van Hove singularities that exist at every band center in the butterfly landscape.

1. Introduction

Discovered by Belgian physicist Leon Van Hove in 1953, Van Hove singularities are singularities in the density of states (*DOS*) crystalline solid [1]. These singularities are known to be responsible for various anomalies provided the Fermi level lies close to such a singularity. Electronic instabilities at the crossing of the Fermi energy with a Van Hove singularity in the DOS often lead to new phases of matter such as superconductivity, magnetism, or density waves [2].

A two-dimensional electron gas (2DEG) in a square lattice provides a simple example of Van Hove singularities in the energy dispersion of a crystal. For a tight binding model of a square lattice the energy dispersion is given by,

$$E = -2J[\cos k_x a + \cos k_y a] \tag{1}$$

Here $\vec{k} = (k_x, k_y)$ is the wave vector in the first Brillouin zone, a is the lattice spacing of the square lattice and J is the nearest-neighbor hopping parameter which defines the effective mass m_e of the electron on the lattice by the relation $J = \frac{\hbar^2}{2m_e a^2}$. This single band Hamiltonian has band edges at $E = \pm 4J$. It can be shown that the DOS at the band edges approaches a constant equal to $\frac{1}{4\pi a^2 \hbar^2}$. However, it diverges at the band center as DOS $\approx \frac{\ln J}{E}$. Such a divergence is an example of a Van Hove singularity. Fig. 1(a) shows the energy contours in (k_x, k_y) plane, where the almost free-electron concentric circles are transformed into a diamond shape structure that corresponds to saddle points in the energy surface. We note that the lattice structure is essential for the existence of Van Hove singularities. Van Hove singularities have been given a topological interpretation in terms of a switching of electron orbits from electron like to hole like [3]. It is worthwhile mentioning that the topological properties of Van Hove singularities in lattices without magnetic fields have been known since long time ago using a theory developed by Morse [4] and applied to solid state physics by J.C. Phillips [5].

In this paper we investigate the Van Hove anomalies of a 2DEG in transverse magnetic fields. Such a system describes all phases of non-interacting electrons as one varies the chemical potential and magnetic field. The phase diagram, known as the Hofstadter butterfly [19] represents various quantum Hall states, each characterized by a quantum number, the Chern number, that has its roots in the nontrivial topology of the underlying Hilbert space [9]. Several aspects of this quantum Hall effect are well understood

* Correspondence to: Departamento de Física–Química, Instituto de Física, Universidad Nacional Autónoma de México (UNAM), Apartado Postal 20-364, 01000 México, Distrito Federal, Mexico.
E-mail address: naumis@fisica.unam.mx.

http://dx.doi.org/10.1016/j.physleta.2016.03.022
0375-9601/

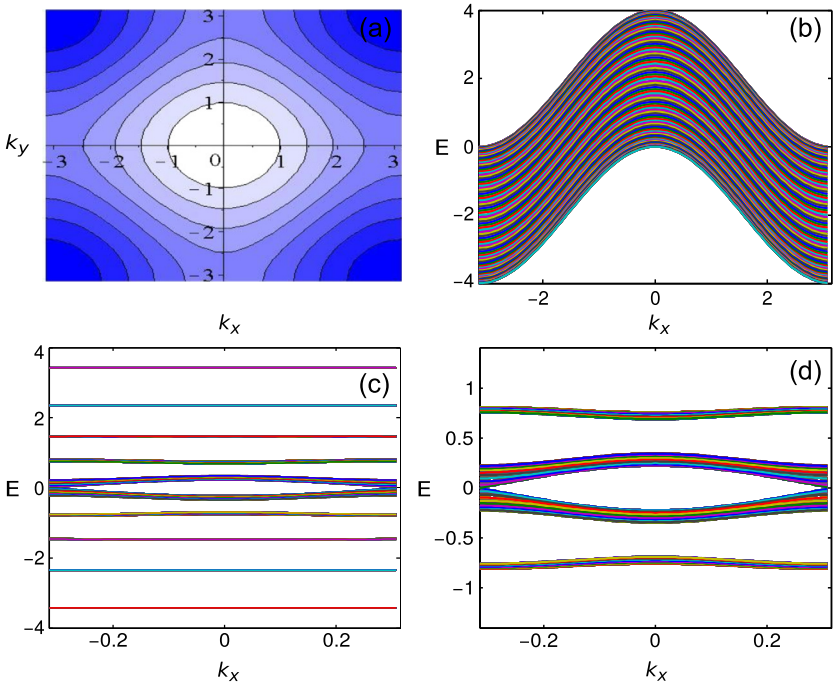

Fig. 1. (a) Contour plot of the energy E in the (k_x, k_y) plane, illustrating the saddle character of the band center for a 2DEG on a square lattice. (b) Shows the corresponding band as a function of k_x. (c) Shows the spectrum for small magnetic flux $\phi = 0.1$. Landau levels correspond to the horizontal flat bands. In (d) we show a blow up of (c) near the band center, illustrating the deviation from the Landau level picture near the band center that hosts a Van Hove singularity. In (b), (c) and (d), the colors represent different values of k_y.

[2] and recently there has been a reemergence of the field due to the first experimental observation of the Hofstadter butterfly [10], leading to perform band-structure engineering [11]. Many of these properties have been measured in graphene over a substrate, since strain in graphene acts as a pseudo magnetic field [12–14]. Also, there is an interest in artificial systems which share the same phenomenology, like ultra cold bosonic atoms [15].

The key result of this paper is the characterization of Van Hove singularities that are nested in the topological hierarchical pattern of the butterfly spectrum. We show that in the two-dimensional energy-flux space, every vicinity of a Van Hove consists of interlacing sequences of Chern numbers. In other words, the Van Hove singularities separate different topological sequences. To achieve this goal, we calculate Chern numbers in the neighborhood of Van Hove singularities, facilitated by simple rules that are derived for determining the entire topological map of the butterfly fractal at all scales.

Notice that there are other previous classic works that studied in detail the layout of the Hofstadter butterfly [16,17] and its relationship with the density of states, however, the fine structure around Van Hove singularities has not been tackled previously. Furthermore, our analysis begins with a simple geometrical approach, based on a method to treat the structure of quasicrystals, that sets the stage for determining the Chern numbers of all the gaps and its associated fine structure. Although this functional relationship is known [18], our geometrical approach allows to find it in a simple way. It also provides a powerful, intuitive and simple geometrical interpretation for the more complicated number theory approach [17]. In fact, we will show that the fine structure of the Hofstadter butterfly can be explained in terms of a simple tilting of the projection subspace used in the cut and projection method.

It is the orderly patterns of topological integers that characterize the fine structure that gets linked to the Van Hove anomalies of a two dimensional crystalline lattice in a magnetic field. Moreover, a very recent study of the 2DEG when subjected to a weak magnetic field, revealed the importance of Van Hove singularities in inducing changes in localization characteristics of the system [6].

In a continuum system, that is, in the absence of any lattice structure, the magnetic field B introduces a magnetic length $l_B = \sqrt{\frac{\Phi_0}{2\pi B}}$ (where Φ_0 is the magnetic flux), reincarnation of the cyclotron radius of the corresponding classical problem. In this limit, the energy spectrum consists of equally spaced harmonic oscillator levels known as the Landau-levels. Interestingly, in a lattice with weak magnetic flux, the Landau level picture breaks down near the band center as illustrated in the Fig. 1. As we will discuss, this is due to the saddle points of the energy dispersion surface. This is in sharp contrast to the parabolic dependence of the energy near the band edges that leads to the Landau levels.

The model system that we study here consists of (spinless) fermions in a square lattice. Each site is labeled by a vector $\mathbf{r} = l\hat{x} + m\hat{y}$, where l, m are integers, and $\hat{x}$ ($\hat{y}$) is the unit vector in the x (y) direction. The tight binding Hamiltonian has the form

$$H = -J_x \sum_{\mathbf{r}} |\mathbf{r} + \hat{x}\rangle\langle\mathbf{r}| - J_y \sum_{\mathbf{r}} |\mathbf{r} + \hat{y}\rangle e^{i2\pi l\phi}\langle\mathbf{r}| + h.c. \tag{2}$$

Here, $|\mathbf{r}\rangle$ is the Wannier state localized at site $\mathbf{r}$. J_x (J_y) is the nearest neighbor hopping along the x (y) direction. With a uniform magnetic field B along the z direction, the flux per plaquette, in units of the flux quantum Φ_0, is $\phi = -Ba^2/\Phi_0$. The field B gives rise to the Peierls phase factor $e^{i2\pi l\phi}$ in the hopping.

Within the Landau gauge, the above Hamiltonian has been engineered in cold atom experiments [7]. Using this gauge, the vector potential is given by $A_x = 0$ and $A_y = -\phi x$ resulting in a Hamiltonian that is cyclic in y. Therefore, the eigenstates of the system can be written as $\Psi_{l,m} = e^{ik_y m}\psi_n$ where ψ_l satisfies the Harper equation [19]

$$\psi_{l+1} + \psi_{l-1} + 2\lambda\cos(2\pi l\phi + k_y)\psi_l = E\psi_l. \tag{3}$$

Here l (m) is the site index along the x (y) direction and $\lambda = J_y/J_x$. For a rational $\phi = p/q$, where p and q are relatively prime integers, the solutions are periodic resulting in the condition $\psi_{l+q} = \exp(k_x q a)\psi_l$.

At the rational flux $\phi = p/q$, the energy spectrum has $q - 1$ gaps, although for even q the central gap is closed. These spectral

gaps are labeled by two quantum numbers which we denote as σ and τ. The integer σ is the Chern number, the quantum number associated with Hall conductivity [9] and τ is an integer. For a Fermi level inside each energy gap, the system is in an integer quantum Hall state [8] characterized by its Chern number σ which gives transverse conductivity $C_{xy} = \sigma \frac{e^2}{h}$ [9].

The quantum number (σ, τ) satisfy a Diophantine equation (DE) [23], that applies to all 2DEG systems that exhibit magnetic translational symmetry,

$$\rho = \phi\sigma + \tau \tag{4}$$

where ρ is the particle density when the Fermi level is in the gap in such a way that $\rho = r/q$. For a given ρ and ϕ, there are infinity of possible solutions for where $[\sigma, \tau]$ are integers, given by,

$$[\sigma, \tau] = [\sigma_0 - nq, \tau_0 + np] \tag{5}$$

Here σ_0, τ_0 are any two integers that satisfy the Eq. (4) and n is an integer. The quantum number σ that determines the quantized Hall conductivity corresponds to the change in the DOS when the magnetic flux quanta in the system is increased by one, whereas the quantum number τ is the change in the DOS when the period of the potential is changed so that there is one more unit cell in the system [24].

For any rational value of the magnetic flux, the system described by the Hamiltonian (2), supports only the $n = 0$ solution of Eq. (5) for the quantum numbers σ and τ. This is due to the absence of any gap closing that is essential for a topological phase transition to states with higher values of σ and τ. However, the DE which relates continuously varying quantities ρ and ϕ with integers σ and τ, has some important consequences about topological changes in close vicinity of rational values of ϕ, as we will discuss in the following sections.

2. Chern numbers and Hull function: a cut and projection quasicrystalline approach

We begin by solving the Diophantine equation, using a geometrical approach well known in the quasicrystal literature – commonly referred as the *Cut and Projection Method* [20,21]. Note that although the explicit solution has been known [18], our approach however illustrates the simplicity underlying the number theoretical approach to solve this equation. The basic idea is to obtain solutions by going to higher dimensions and the required solutions are the projections from two to one dimension.

We start by defining two vectors: a flux vector $\boldsymbol{F}$ and a topology vector $\boldsymbol{T}_r$ as,

$$\boldsymbol{F} = (p, q), \qquad \boldsymbol{T}_r = (\sigma_r, \tau_r) \tag{6}$$

The DE is then rewritten as,

$$r = \boldsymbol{F} \cdot \boldsymbol{T}_r \tag{7}$$

This implies that the gap index r is a projection of the topology vector onto the flux vector. However, this projection is an integer. This suggests the following scheme to obtain the components of $\boldsymbol{T}_r$, namely σ_r, τ_r in terms of r as follows.

As shown in Fig. 2, we consider a two dimensional space with coordinates (x, y). A square lattice is defined in this space by considering x and y at integer values.

A vector $\boldsymbol{F}$ is drawn which points to the square lattice point (p, q). Then all possible solutions of the Diophantine lay in the 2D square lattice, and are contained in a family of parallel lines given by,

$$r = (p, q) \cdot (x, y) \tag{8}$$

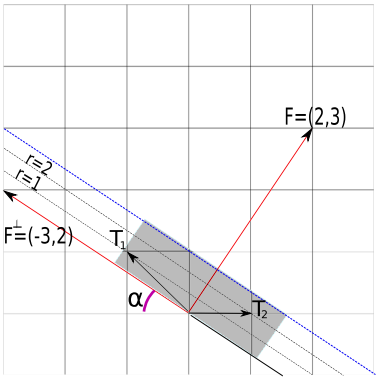

Fig. 2. Geometry associated with the cut and projection method to obtain the solutions of the Diophantine equation. In this example, the flux is chosen to be $\phi = 2/3$. The set of parallel lines gives the solutions for each gap r. Two solutions are shown here, $\boldsymbol{T}_1 = (-1, 1)$ and $\boldsymbol{T}_2 = (1, 0)$.

as indicated in Fig. 2. To find integer solutions, we look at the family of parallel lines. These lines are all parallel to the vector,

$$\boldsymbol{F}^{\perp} = (-q, p) \tag{9}$$

which defines the line $y = -\phi x$, with slope $\phi = \tan\alpha$ where α is the angle between the x axis and $\boldsymbol{F}^{\perp}$. If x is chosen to be an integer, that we associate with a Chern number σ_r, this will produce a y coordinate,

$$y = -\phi\sigma_r \tag{10}$$

However, although y is in the family of parallel lines that contains all solutions, only integer values of y are required by the Diophantine equation. To find such integers, we just take the floor function of the previous equation,

$$\lfloor y \rfloor = -\lfloor \phi\sigma_r \rfloor \tag{11}$$

so for each σ_r, the corresponding τ_r is given by,

$$\tau_r = -\lfloor \phi\sigma_r \rfloor \tag{12}$$

Thus, gaps are labeled by the coordinates of a two dimensional lattice,

$$(\sigma_r, \tau_r) = (\sigma_r, -\lfloor \phi\sigma_r \rfloor) \tag{13}$$

Furthermore, by using the identity $x = \lfloor x \rfloor + \{x\}$ to express τ_r and inserting the solution into Eq. (7), we obtain a relationship between the filling fraction r/q and the Chern numbers,

$$\frac{r}{q} = \{\phi\sigma_r\} \tag{14}$$

Notice that care must be taken for negative Chern numbers, since $\{-x\} = 1 - \{x\}$ for $x > 0$. To be more specific, now we define the *Hull function* f as,

$$f(\phi, \sigma) = \{\phi\sigma_r\} \tag{15}$$

which is the filling factor for a Chern number at a given ϕ.

This formula can be inverted using the same methodology giving the Chern numbers as a function of the gap index,

$$\sigma_r = q\left\{\phi r + \frac{1}{2}\right\} - \frac{q}{2} \tag{16}$$

As an example of how to use Eq. (16), consider the case $\phi = 4/5$. For the first gap $(r = 1)$ we have,

$$\sigma_1 = 5\left\{\frac{4}{5} + \frac{1}{2}\right\} - \frac{5}{2} - = 5\left(\frac{3}{10}\right) - \frac{5}{2} - = -1 \tag{17}$$

It is easy to verify that using $\tau_1 = 1$, the obtained solution satisfies the Diophantine for $r = 1$, e.g., $\rho = 1/5 = -4/5 + 1$. Following a

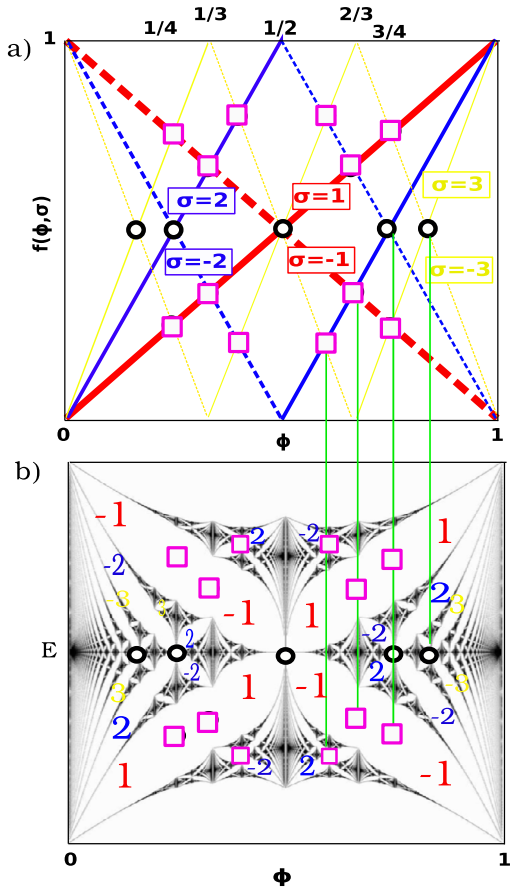

Fig. 3. The skeleton (panel (a)) and the butterfly graph with the gaps labeled with its Chern numbers (panel (b)). The skeleton shows the function $f(\sigma,\phi)$ as a function of ϕ for the Chern numbers $\sigma=\pm1$ (red), $\sigma=\pm2$ (blue) and $\sigma=\pm3$ (yellow). Positive Cherns correspond to solid lines and negative Cherns are broken lines. Chern number intersections are marked with circles and boxes, and some of the intersection values are labeled at the top of the panel. The pattern and meetings of Chern numbers in the skeleton have a correspondence in the butterfly plot, as indicated in some cases by vertical lines from panel (a) to panel (b). The circles indicate butterfly centers in which the Chern numbers meet their negative counterparts, while the boxes are meetings that do not have this property. (For interpretation of the references to color in this figure legend, the reader is referred to the web version of this article.)

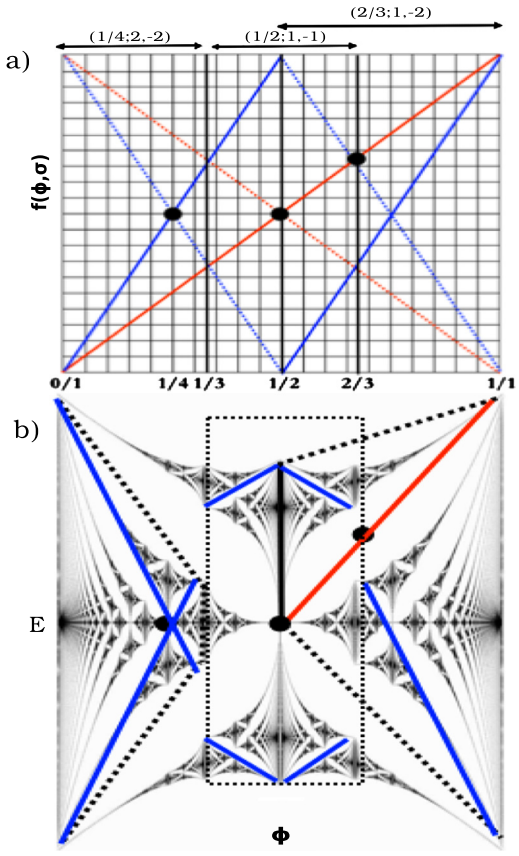

Fig. 4. The skeleton (panel (a)) and the butterfly graphs (panel (b)), showing explicitly the Cherns ±1 (red) and ±2 (blue) as a function of ϕ. Positive Cherns are solid lines and negative Cherns are broken lines. In addition to the entire butterfly, we identify three butterflies in the graph, whose centers are shown with black dots and are marked in the bottom graph with a trapezoid or a rectangle. The lines in panel (b) are guides to the eye going along the butterflies wings. The bottom butterfly graph in panel (b) shows these butterflies enclosed inside the trapezoids: one with meeting Chern numbers 2 and -2 centered at $\phi=1/4$, the other with Chern numbers 1 and -2 centered at $2/3$. In addition, there is another butterfly enclosed in a rectangle, centered at $1/2$. The corresponding flux values for these three different butterflies are also shown with double arrowed lines that are labeled by the flux and the two values of the meeting Cherns. Notice that the upper left wing of the butterfly centered at $\phi=2/3$ coincides with one of the wings of the butterfly centered at $\phi=1/2$. The butterfly centered at $\phi=1/2$ has two wings in the low-energy region and the other two in the high-energy region. (For interpretation of the references to color in this figure legend, the reader is referred to the web version of this article.)

similar procedure, we find the other Cherns numbers, $\sigma_2=-2$, $\sigma_3=2$, $\sigma_4=1$ and its corresponding partners $\tau_2=2$, $\tau_3=-1$ and $\tau_4=0$.

Notice that the ordering of the gaps coincides with the ordering in energy since the filling fraction ρ, which gives the position of the Fermi energy, is proportional to r.

3. Butterfly topological map: Chern meeting formula and fine structure

The hull function [22] can be viewed as a kind of "skeleton butterfly" plot that encodes the topological structure of the Hofstadter spectrum as we explain below. Earlier studies have discussed this skeleton in terms of the integrated density of states, and not in terms of its topological properties [16]. In this paper, we use this Hull function along with the numerically obtained butterfly to lay out the topological patching of the entire butterfly. Upper and lower graphs in Fig. 3 illustrate the relationship between the topology of the butterfly graph and its skeleton version obtained from the Hull function. We emphasize that although the quantitative analysis of the actual energies requires a numerical exploration, many features can be obtained using the Hull function. As we discuss below, this includes not only the dominant gaps but the fine structure associated with them. Fig. 3 shows the filling fractions $r/q=f(\phi,\sigma)$ as a function of flux ϕ for Chern numbers $\pm1,\pm2$ and ±3. Notice that for a fixed σ, $f(\phi,\sigma)$ is just a saw-tooth function with $|\sigma|$ distinct branches when considering for ϕ between 0 and 1. The intersection of two branches are points where distinct Cherns meet as indicated in Fig. 3(a). In the butterfly spectrum, the meetings of branches is reflected in meeting of gaps, as seen in Fig. 3(b).

We now identify a "central butterfly" and its fine structure as follows. As shown in Fig. 4, consider again $f(\phi,\sigma)$ as a function of ϕ for some different values of σ. In the plot we present as an example $f(\phi,1)$, $f(\phi,-1)$, $f(\phi,2)$ and $f(\phi,-2)$. The intersections of $f(\phi,\sigma)$ for different σ will occur for some fluxes. Each intersection defines the center of a butterfly. However, at each intersection there are also many other Cherns that meet. Then we associate a central butterfly with the meeting of the two smallest Cherns (in magnitude) which meet at a certain ϕ. The other Cherns that converge at the same point will be identified with the fine structure of this central butterfly, as we will explain later. As an example, consider the lowest Cherns $\sigma=1$ and $\sigma=-1$. In Fig. 4 they produce

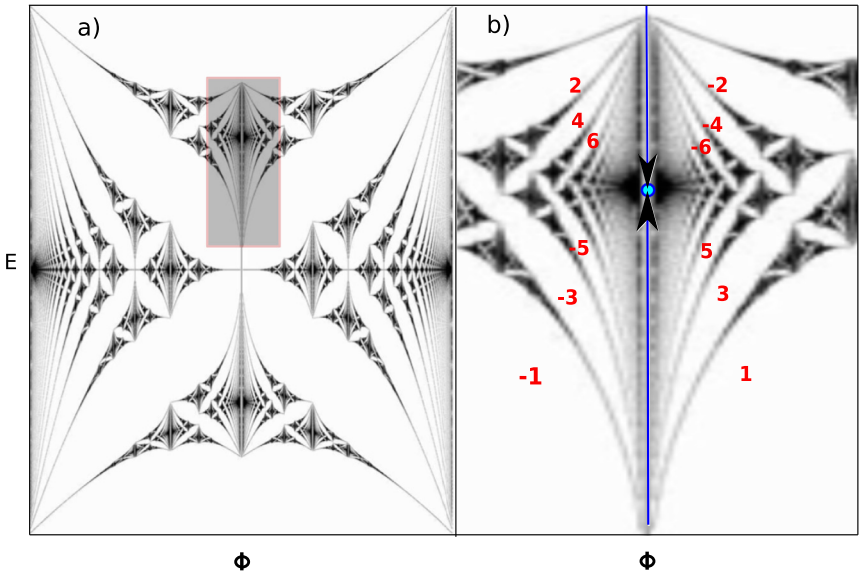

Fig. 5. An example of the butterfly fine structure, showing the topological sequences around a singularity. In panel (b) we present a zoom of the boxed region of the butterfly shown in panel (a). The zoom shows the sequences of Chern numbers around the flux $\phi = 1/2$. Four sequences are observed, given by odd and even Chern numbers and its negative counterparts. The sequences "collide" as the arrows indicate. The collision point is indicated by a circle and corresponds to a Van Hove singularity.

two functions corresponding to $f(\phi, 1)$ and $f(\phi, -1)$. These two functions intersect at $\phi = 1/2$. This turns out the be the center of the biggest butterfly in the spectrum, where the size is adscribed by looking at the length of the wings. At the same time, for $\phi = 1/2$ there are other Chern meetings, as for example the intersections of $f(\phi, 3)$ and $f(\phi, -3)$ as indicated in Fig. 3. These and other higher Chern meetings at $\phi = 1/2$, as well as the discontinuities of $f(\phi, \sigma)$ at $f = 0$ and $f = 1$, are responsible of the fine structure, leading to a collapse of Cherns and its associated Van Hove singularity. As seen in the bottom panel of Fig. 4, the main structure of the spectrum can be easily understood by studying the structure of the Chern meetings.

Cherns meetings are not arbitrary. To see this point, let us consider two gaps in the butterfly landscape, one with gap index $r = a$ and Chern number σ_a, and another with gap index $r = b$ and Chern σ_b, both emanating from the left of the graph and meeting at a certain $\phi = p/q$. These two gaps will exchange their corresponding value of r at the meeting point. Thus, in the vicinity of the meeting point we get from the Hull function that,

$$\lim_{\delta\phi \to 0^-} \{(\phi - \delta\phi)\sigma_a\} = \lim_{\delta\phi \to 0^+} \{(\phi - \delta\phi)\sigma_b\} \tag{18}$$

This equation can only be satisfied provided,

$$q = \sigma_a - \sigma_b \tag{19}$$

since the fractional part function has period 1 and $\{x\} = x$ for $0 \leq x < 1$, i.e., when applied to this particular case, $\{\phi\sigma\} = \{(p/q)\sigma\} = (p/q)\sigma$ and the period is q. In principle, the arguments of the fractional parts in Eq. (18) can differ up to any multiple of the period, however, Chern numbers are between $-q/2$ and $q/2$ leaving only one possibility in Eq. (19).

This equation, which we will refer as the *Chern meeting formula*, relates the topological quantum numbers of two swaths of the butterfly that meet at a point. The most simple example is the following one. Chern numbers $\sigma_a = -1$ and $\sigma_b = 1$ will have $q = 2$ from where the meeting is at $\phi = 1/2$. Chern numbers $\sigma_a = -2$ and $\sigma_b = 2$ will have $q = 4$ from where the meetings are at $\phi = 1/4$, $\phi = 1/2$ and $\phi = 3/4$. From this example, we learn something important. Meetings at $\phi = 1/4$ and $\phi = 3/4$ correspond to the center of butterflies, while the meeting for $\phi = 1/2$ corresponds to a kind of fountain seen at the center, as shown in Fig. 5. As we will see

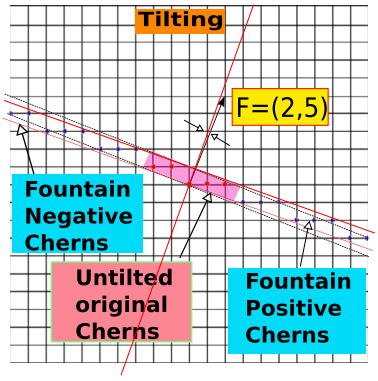

Fig. 6. Tilting around a given flux, in this case $\phi = 2/5$. The corresponding flux vector is indicated with an arrow, and the projection space is shown with doted lines. The shaded region contains the solutions of the Diophantine equation for $\phi = 2/5$, indicated by red circles. Notice that in principle, other solutions exists due to the periodicity of the Diophantine equation solutions, however, they are equivalent to those inside the shaded region, determined by Cherns between $-q/2$ and $q/2$. By tilting by a small angle, new solutions appear as indicated by indigo circles inside the solid lines. These new solutions produce topological sequences identified with "fountain" structures. For $x > 0$, the sequence is made from positive Cherns numbers, while for $x < 0$ is made with negative Chern numbers. (For interpretation of the references to color in this figure legend, the reader is referred to the web version of this article.)

below, this particular meeting is part of the fine structure of the butterfly which contains several topological sequences. In other words, for $\phi = 1/2$, we have that $q = 2$ and any Cherns that satisfy $\sigma_a - \sigma_b = 2$ will appear, as seen in Fig. 5. Therein, we see four cascades of meeting gaps, characterized by upper and lower sets of Cherns, forming a kind of fountains with fountainheads located at $E = 0$ and $E_{\max}$. For fluxes $\phi > 1/2$, one sequence is $1, 3, 5, 7, \ldots$ and the other $-2, -4, -6, \ldots$. Both sequences seem to "collide" in the circle indicated in Fig. 5, which eventually we will associate with a Van Hove singularity.

These topological sequences, that we call the fine structure, are easy to understand from the quasicrystalline approach. If for a given flux ϕ we perform a small tilting $\delta\alpha$ of the angle α leading to a new flux $\phi + \delta\phi$, then a cascade of new solutions to the Diophantine arise, as shown in Fig. 6 for the particular case

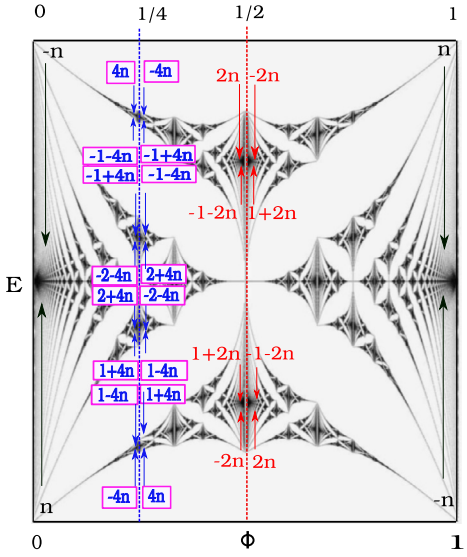

Fig. 7. Labeling of some gaps with the Chern number sequences obtained by using Eq. (21) and Eq. (24) for fluxes around the indicated values at the top of the plot. These topological sequences in the butterfly spectrum are what we call the fine structure. Notice that Landau levels near $\phi = 0$ and $\phi = 1$ also form a sequence. The sequence of negative and positive Landau levels is separated by the Van Hove singularity of the square lattice without an applied magnetic field.

$\phi = 2/5$. Clearly, for any rational flux we can tilt to obtain these sequences.

The tilting argument can be made rigorous as follows. Suppose that we tilt a $\phi_0 = p_0/q_0$ to $\phi = \phi_0 + \delta\phi$. Then the Chern numbers must change to $\sigma = \sigma_0 + \delta\sigma$, and the Hull function goes to

$$\frac{r}{q} = \left\{ (\frac{p_0}{q_0} + \delta\phi)(\sigma_0 + \delta\sigma) \right\} \tag{20}$$

However, $\delta\sigma$ must be an integer even when $\delta\phi \to 0$. The only general way to satisfy this condition is to have that $\delta\sigma = \pm nq_0$ where n is a positive integer. Thus, the new Cherns are,

$$\sigma = \sigma_0 \pm nq_0 \tag{21}$$

These are precisely the "fountain" sequences observed around rational fluxes. The above condition determines the entire topological map of the butterfly as described in Fig. 7. This plot illustrates the fine structure in the entire butterfly landscape by showing the sequences of Cherns numbers.

However, one must be careful in applying Eq. (21) since the chosen value of $\delta\phi$ puts a limit on the maximal allowed value of n. Geometrically, the reason is evident since for the new rational flux $p/q = \phi_0 + \delta\phi$ there is a new periodicity in the solutions determined by q, as can be observed in Fig. 6 when the red solid lines hit a point of the mesh. From the point of view of the Hull function, this is also easy to see by calculating the period. In fact, at the end of the next section we will provide an expression for the maximal n. When n is lower than this limit, we can use that for two numbers a and b, we have that $\{a + b\} = \{a\} + \{b\}$ as long as $\{a\} + \{b\} < 1$. Thus, from Eq. (20) we have that for $\delta\phi > 0$ the filling fraction is,

$$f(\phi, \sigma) = f(\phi, \sigma_0) \pm nq_0\delta\phi \tag{22}$$

where careful has to be taken in this demonstration when $\sigma = \sigma_0 - nq_0$ as well as for negative $\delta\phi$, due to the definition of the fractional part for negative numbers. When $\delta\phi \to 0$, Eq. (22) can be further simplified by observing that,

$$\lim_{\delta\phi\to 0} f(\phi, \sigma_0) = f(\phi_0, \sigma_0) + \lim_{\delta\phi\to 0} \{\sigma_0\delta\phi\} = f(\phi_0, \sigma_0) \tag{23}$$

Using this previous result in Eq. (22) we obtain the filling ratio for the topological sequence,

$$f(\phi, \sigma) \approx f(\phi_0, \sigma_0) \pm nq_0\delta\phi \tag{24}$$

According to Eq. (24), the filling fraction increases linearly with n if $n > 0$ and $\delta\phi > 0$. For example, if $\phi_0 = 1/2$ and $\sigma_0 = 1$, this leads to a sequence $3, 5, 7, \ldots$ which grows in energy for $\phi > 1/2$ as seen in Fig. 5. In the same Fig. 5, the sequence $-2, -4, -6, \ldots$ decreases in energy as expected. To the left of $\phi = 1/2$, i.e., $\delta\phi < 0$, we see that the sequence $-1, -3, -5$ increases in energy as predicted from Eq. (22). In Fig. 7 we present other topological sequences around different values of ϕ in which this rule is observed for other topological sequences of the fine structure. It is worthwhile to observe that Landau levels are obtained from the sequence for $q = 1$, leading to the sequence $2, 3, 4, 5, \ldots$ and $-2, -3, -4, \ldots$. The first of these sequences grows in energy while the other decreases near $\phi = 0$, while the order is inverted near $\phi = 1$. This interchange is due to the tilting with a negative or positive $\delta\alpha$ around $\alpha = 0$.

4. Van-Hove singularities as limits for the topological sequences

Having determined the topological structure of the butterfly landscape where the gaps have been the focus of our discussion, we now turn our attention to some interesting characteristics of the bands. We show that the fine structure of the gaps discussed earlier are rooted in Van Hove singularities that reside at the band center. In the presence of a magnetic flux p/q, a single band is split into q-bands. The center of each of this sub-band exhibits a Van Hove singularity. Therefore, accompanying the hierarchical set of bands in the butterfly landscape are also a set of Van Hove singularities, seen just with an eye blink, as dark spots – that is, high density points. In fact, the low magnetic flux limit discussed in the beginning applies to the neighborhood of every rational flux.

Fig. 8 illustrates the Van Hove singularities in the fragmented DOS in the presence of a magnetic field. This clearly shows that Van Hove are integral part of *every* band center, irrespective of its location in energy. In other words, no matter how fragmented a band is, its center is always a critical point that hosts a Van Hove singularity. In the case of incommensurate flux where bands have zero measure as the width of every band approaches zero, the surviving Cantor set or "dust" encodes a fractal set of Van Hove singularities, as it has been seen in a multifractal analysis of the spectrum [25]. The Fig. 8 shows versions of the butterfly DOS between fluxes 1/3 and 2/5. The zoom for $\phi = 11/30$ in Fig. 8(d) shows that the central band is a scaled version of the case $\phi = 1/2$, as shown in Fig. 8(a).

We next address the question of how the topology of the butterfly is influenced by the Van Hove singularities. Fig. 9 shows the topological landscape in the vicinity of some Van Hove singularities, illustrating panel (b) what happens to the zero-field Van Hove as the system is subjected to a small magnetic flux ϕ. The magnetic field that fragments the band and the resulting cascade of channels or gaps are characterized by positive and negative Cherns interlaced as illustrated in the figure. Again, this type of behavior is present at all band centers. For example, Fig. 9(c) shows the Van Hove singularity indicated by B on 9 panel (a) and the topological landscape in its neighborhood at $\phi = 1/2$. Van Hove singularities marked as B and C in Fig. 9(a) at $\phi = 1/2$ are replicas of singularity A for $\phi = 0$, were by replicas we mean that the shape of the singularity is the same, but a scaled width and height.

Note that the sequence of Cherns near the Van Hove are the higher order solutions of the Diophantine equation, described in Eq. (21). This brings us to an interesting point about the importance of these topological states that are accumulated around the Van Hove. To gain further understanding on this accumulation,

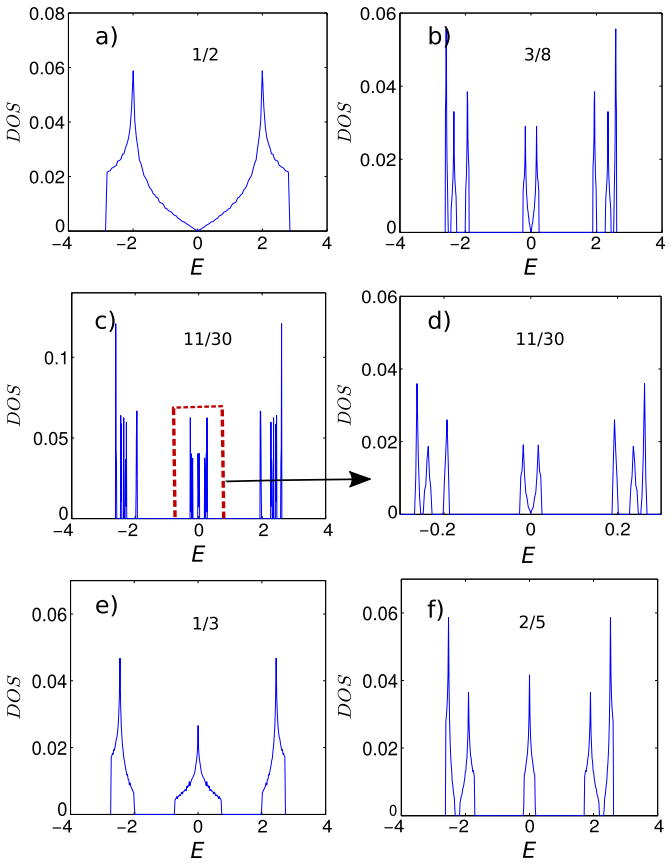

Fig. 8. (Color online.) DOS as a function of the energy for several fluxes. Panel (a) corresponds to flux $\phi = 1/2$, (b) to $\phi = 3/8$, (c) to $\phi = 11/30$, (e) to $\phi = 1/3$ and (f) to $\phi = 2/5$. Panel (d) is a zoom for $\phi = 11/30$ in the region indicated by the box in panel (c). This plot illustrates how Van-Hove singularities exist at every band, irrespective of its location in flux value and energy. Furthermore, they form self-similar patterns. For odd q, the central band is a scaled version of the square lattice, as shown here for $\phi = 1/3$ and $\phi = 2/5$

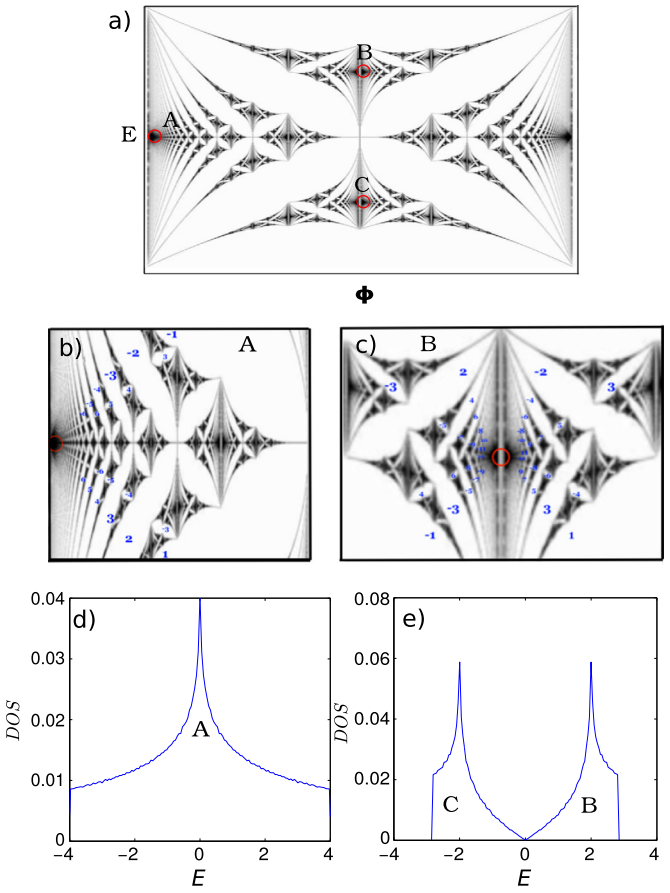

Fig. 9. (Color online.) Illustrating the topological collapse near a Van-Hove singularity. In panel (a), the circles (red) show three Van Hove singularities in the butterfly, labeled by A, B and C. In panels (b) and (c), a sequence of cascades of gaps with both positive and negative Cherns annihilate around the points A and B respectively. Finally, in (d) we present the DOS for $\phi = 0$. The peak at the Van Hove singularity at $E = 0$ corresponds to point A. In (e), we present the DOS for $\phi = 1/2$. The peaks at $E = 2$ and $E = -2$ correspond to the Van Hove singularities identified with the points B and C of the butterfly shown in panel (a).

consider the case $\phi = 0$. As seen in Fig. 9(d), there is a Van Hove singularity at the center, as is well known for a square lattice without a magnetic field. Now we add a small tilting of the flux to $\phi = 1/50$. In Fig. 10(a) we present the resulting DOS calculated using bins in energy which are small enough to resolve all the bands (an alternative procedure is to modify the small imaginary part added at the poles of the Green's function). At the band edges, one can see equally spaced levels while at the center there is an accumulation of states. The equally spaced states are the Landau levels. If the resolution in energy is decreased as seen in 10(b), the states near the center merge in a peak leading to a kind of Van Hove singularity, while Landau levels remains at the edges. Physically, states near the Van Hove singularity are different from Landau level states. Near the Van Hove singularity, the level spacing is reduced, as pointed out by Hsu and Falicov [26], for all practical purposes the subbands merge in an almost continuous band near the saddle points, as seen in Fig. 10. When the flux is slightly perturbed, there is a mixing between these states, which is not the case for the Landau levels. As a result, the bands as a function of k_x are not flat as it happens with the Landau levels, as seen in Fig. 1(c) and (d) by tilting from $\phi = 0$ to $\phi = 1/10$. Clearly, the localization properties of Landau states are very different from the ones near the Van Hove singularity due to the curved character of the band, i.e., the effective mass is not infinity as it is for the Landau levels.

Now that the numerical connection between the Van Hove singularity and the fine structure of the butterfly has been established, is time to derive it from the Hamiltonian. We start by using the observation made by Thouless [27] that due to the duality of the resulting Harper equation for the Hamiltonian given by Eq. (2), the wave vectors will enter in the energy dispersion in the form $E(k_x, k_y) = E(\xi(k_x, k_y))$ where $\xi(k_x, k_y)$ is given by [27],

$$\xi(k_x, k_y) = -2\cos(k_x qa) - 2\cos(k_y qa) \tag{25}$$

From this, Thouless [27] showed that the band edges are the extremal values of $\xi(k_x, k_y)$, which are given by the center of the magnetic lattice Brillouin zone $\mathbf{\Gamma} = (0, 0)$ and the points $\mathbf{X} = (\pi/qa, \pi/qa)$ and $\mathbf{X}' = (\pi/qa, -\pi/qa)$. The energies associated with the $\mathbf{\Gamma}$ point are the lower band edges while the points $\mathbf{X}$ and $\mathbf{X}'$ give the upper band edges. Since we have two extremal values in a periodic function, this automatically implies the existence of a third singularity [4]. This singularity occurs when the derivative of $E(k_x, k_y)$ changes sign [4]. In the present case, since the energy dispersion depends on $\xi(k_x, k_y)$, a singularity in this function will produce a singularity on $E(k_x, k_y)$ due to the chain rule for the derivative. Thus, since we have that

$$\nabla_{\mathbf{k}} \xi(k_x, k_y) = 2qa(\sin(k_x qa), \sin(k_y qa)) \tag{26}$$

$E(k_x, k_y)$ has saddles at two inequivalent points in the magnetic Brillouin zone, given by $\mathbf{M} = (0, \pi/qa)$, $\mathbf{M}' = (\pi/qa, 0)$. In such points, the energy dispersion will look as [4],

$$E(k_x, k_y) = \pm A k_x^2 \mp B k_y^2 \tag{27}$$

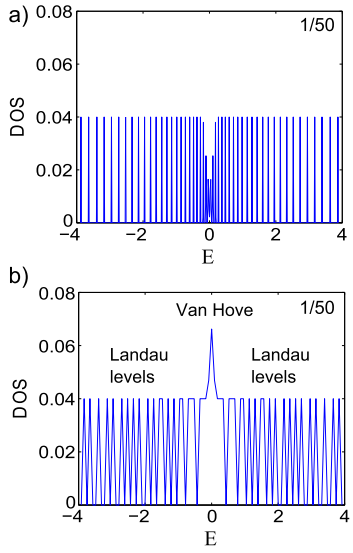

Fig. 10. (Color online.) The DOS as a function of the energy for $\phi = 1/50$, i.e., near the flux $\phi = 0$. In panel (a) we show the DOS with a resolution grid in E of 600 bins, able to resolve all the 50 bands. Notice how the distance between levels decreases near $E = 0$. In panel (b), the resolution is changed to 90 bins in E. With this resolution, the spectrum seems to be made from a Van Hove singularity with Landau levels at the edges. A comparison with Fig. 9(d) for the case $\phi = 0$, shows how the Van Hove singularity arises.

where A and B are constants. This energy dispersion can be integrated to get a DOS which diverges in a logarithm form [4] for any band s,

$$\rho(E) = C \log(E - E_s^{VH}(\phi)) \tag{28}$$

with C a constant and $E_s^{VH}(\phi) = E_s(k_x, \pm k_x \pm \pi/qa)$, corresponding to the energy associated with states along the edges of a nested square in the magnetic Brillouin zone. This nested square has the points **M** and **M**′ as its corners. This shows that there is a Van Hove logarithm divergence at each band of the spectrum.

Let us connect this result with the topological sequences. Along the edges of the nested square $\xi(k_x, k_y)$ has a separatrix. States inside the nested square will have energies $E < E_s^{VH}$ while states outside have $E > E_s^{VH}$. Since the area of the nested square is equal to the sum of the areas that are outside the square, is clear that we have as many states for $E > E_s^{VH}$ as for $E < E_s^{VH}$. From this, it follows that the Van Hove singularities arise at half filling of each band, i.e., we can write that,

$$f^{VH} = \frac{r}{q} + \frac{1}{2q} \tag{29}$$

where f^{VH} is defined as the filling fraction at the Van Hove singularity. Notice that the structure described for the Brillouin zone is basically the same that appears in the particular case $\phi = 0$ shown in Fig. 1(a), where negative energies are obtained for states inside the square with corners $(0, \pm\pi)$ and $(\pm\pi, 0)$, while positive values correspond to states outside the square.

Now we observe that Eq. (24) provides the filling fraction for the limit of the topological sequences. Consider a band limited by gaps r and $r+1$ for a flux $\phi = p/q$. Consider also the topological sequences starting from the bottom and top of the band by tilting by a small $\delta\phi$. Using Eq. (24), the filling fractions for the sequence that starts at the bottom are given by,

$$f(\phi + \delta\phi, \sigma_{r+n}) \approx \frac{r}{q} + nq\delta\phi \tag{30}$$

while the sequence that starts from the top is,

$$f(\phi + \delta\phi, \sigma_{r+1-n}) \approx \frac{r+1}{q} - nq\delta\phi \tag{31}$$

The difference in filling fraction between both sequences is,

$$f(\phi + \delta\phi, \sigma_{r+1-n}) - f(\phi + \delta\phi, \sigma_{r+n}) \approx \frac{1}{q} - 2nq\delta\phi \tag{32}$$

However, the sequences cannot cross one over the other, this requires that the previous quantity must be bigger or equal to zero,

$$\frac{1}{q} - 2nq\delta\phi \geq 0 \tag{33}$$

From the previous equation we found the relationship between n and $\delta\phi$,

$$n\delta\phi \leq 1/2q^2 \tag{34}$$

which provides a limiting n, denoted by n_{Max}, for a given $\delta\phi$,

$$n_{Max}\delta\phi = 1/2q^2 \tag{35}$$

This value can be used in Eq. (30) to obtain,

$$\lim_{\delta\phi\to 0} f(\phi + \delta\phi, \sigma_{r+n_{Max}}) = \frac{r}{q} + \frac{1}{2q} \tag{36}$$

Comparing Eqs. (29) and (36), is clear that,

$$f^{VH} = \lim_{\delta\phi\to 0} f(\phi + \delta\phi, \sigma_{r+n_{Max}}) \tag{37}$$

and thus the Van Hove singularity is at the limit for the topological sequences. This result explains the numerically observed topological collisions at the Van Hove singularities.

5. Conclusions

In summary, the topological characterization of the butterfly landscape can be described by a topological map of the butterfly built from a method taken from quasicrystals, the cut and projection method. This map provide rules for the spectrum, i) the butterflies are determined by a Chern meeting formula, ii) around any rational flux, there is a fine structure made from sequences of Chern numbers, iii) the topological sequences are separated by Van Hove singularities. In fact, such singularities carry a lot of the spectral weight and thus are the most visible features when small disorder is added to the problem [19].

Finally, the present work points in the direction of finding a common ground for the description of quasicrystals and the quantum Hall effect [28]. For example, the fine structure of the quantum Hall spectrum is similar to the one obtained by phason satellites that appear in electron diffraction for quasicrystals [29–32].

Acknowledgements

I would like to thank a PASPA-DGAPA UNAM sabbatical scholarship to spend a semester at George Mason and acknowledge George Mason University for the hospitality. This work was partially funded by UNAM DGAPA-PAPIIT proyect 102513. Also, I would like to thank Indu Satija for discussions on the subject, and D. Hofstadter for inspiring talks concerning the history of the G-plot spectrum, nowadays known as the Hofstadter butterfly.

References

[1] L. Van Hove, The occurrence of singularities in the elastic frequency distribution of a crystal, Phys. Rev. 89 (1953) 1189–1193.
[2] E. Fradkin, Field Theories of Condensed Matter Physics, 2nd edition, Cambridge University Press, Cambridge, 2013.
[3] R.S. Markiewicz, J. Phys. Condens. Matter 6 (1994) 3035.
[4] W. Jones, N.E. March, Theoretical Solid State Physics, Vol. 1: Perfect Lattices in Equilibrium, Dover, New York, 2001.
[5] J.C. Phillips, Phys. Rev. 104 (1956) 1263.
[6] Yi Zhang, Daniel Bulmash, Akash V. Maharaj, Chao-Ming Jian, Steven A. Kivelson, arXiv:1504.05205 [cond-mat.dis-nn], 2015.

[7] Y.-J. Lin, et al., Phys. Rev. Lett. 102 (2009) 130401;
D. Hofstadter, I.B. Spielman, Phys. Rev. A 79 (2009) 063613.
[8] Y. Hatsugai, Phys. Rev. Lett. 71 (1993) 3697.
[9] D.J. Thouless, M. Kohmoto, M.P. Nightingale, M. den Nijs, Phys. Rev. Lett. 49 (1982) 405.
[10] C.R. Dean, L. Wang, P. Maher, C. Forsythe, F. Ghahari, Y. Gao, J. Katoch, M. Ishigami, P. Moon, M. Koshino, T. Taniguchi, K. Watanabe, K.L. Shepard, J. Hone, P. Kim, Nature 497 (2013) 598?602.
[11] B. Hunt, J.D. Sanchez-Yamagishil, A.F. Young, M. Yankowitz, B.J. LeRoy, K. Watanabe, T. Taniguchi, P. Moon, M. Koshino, P. Jarillo-Herrero, R.C. Ashoori, Science 340 (2013) 6139.
[12] M. Oliva-Leyva, G.G. Naumis, Phys. Rev. B 88 (2013) 085430.
[13] Pedro Roman-Taboada, Gerardo G. Naumis, Phys. Rev. B 90 (2014) 195435.
[14] Gerardo G. Naumis, Pedro Roman-Taboada, Phys. Rev. B 89 (2014) 241404(R).
[15] M. Aidelsburger, M. Lohse, C. Schweizer, M. Atala, J.T. Barreiro, S. Nascimbène, N.R. Cooper, I. Bloch, N. Goldman, Nat. Phys. 11 (2014) 162.
[16] F.H. Claro, W.H. Wannier, Phys. Rev. B 19 (1979) 6068–6074.
[17] D. Osadchy, J.E. Avron, J. Math. Phys. 42 (2001) 5665.
[18] P.B. Wiegmann, Prog. Theor. Phys. Suppl. 34 (1999) 171–181.
[19] D. Hofstadter, Phys. Rev. B 14 (1976) 2239.
[20] D. Levine, P.J. Steinhardt, Phys. Rev. B 34 (1986) 596.
[21] C. Janot, Quasicrystals, 2nd ed., Clarendon, Oxford, 1994.
[22] G.G. Naumis, J.L. Aragón, Z. Kristallogr. 208 (2003) 1.
[23] I. Dana, Y. Avron, J. Zak, J. Phys. C, Solid State Phys. 18 (1985) L679.
[24] Allan Mac-Donald, Phys. Rev. B 28 (1983) 67136717.
[25] M. Kohmoto, Phys. Rev. B 34 (1986) 2041.
[26] W.Y. Hsu, L.M. Falicov, Phys. Rev. B 13 (1976) 1595.
[27] D.J. Thouless, Phys. Rev. B 28 (1983) 4272.
[28] G.G. Naumis, F.J. López-Rodríguez, Physica B 403 (2008) 1755–1762.
[29] J.C. Lopez, G. Naumis, J.L. Aragon, Phys. Rev. B 48 (1993) 12.
[30] G.G. Naumis, Phys. Rev. B 59 (1999) 11315.
[31] G.G. Naumis, Ch. Wang, M.F. Thorpe, R.A. Barrio, Phys. Rev. B 59 (14) (1999) 302.
[32] G.G. Naumis, Phys. Rev. B 71 (2005) 144204.